Supplementary Information

Codoping Er-N to suppress self-compensation donors for stable *p*-type zinc oxide

Yifang Ouyang[1], Zhisen Meng[1], Xiaoming Mo[1], Hongmei Chen[1], and Xiaoma Tao[1,*], Qing Peng[2,*], Yong Du[3]

[1] College of Physical Science and Technology, Guangxi University, Nanning, Guangxi 530004, People's Republic of China

[2] Department of Nuclear Engineering and Radiological Science, University of Michigan, Ann Arbor, MI48109, USA

[3] State Key Laboratory of Powder Metallurgy, Central South University, Changsha, Hunan 410083, People's Republic of China

[*] Corresponding emails: taoxiaoma@gxu.edu.cn(X.T.) qpeng.org@gmail.com (Q.P.)

1. Formation Energy

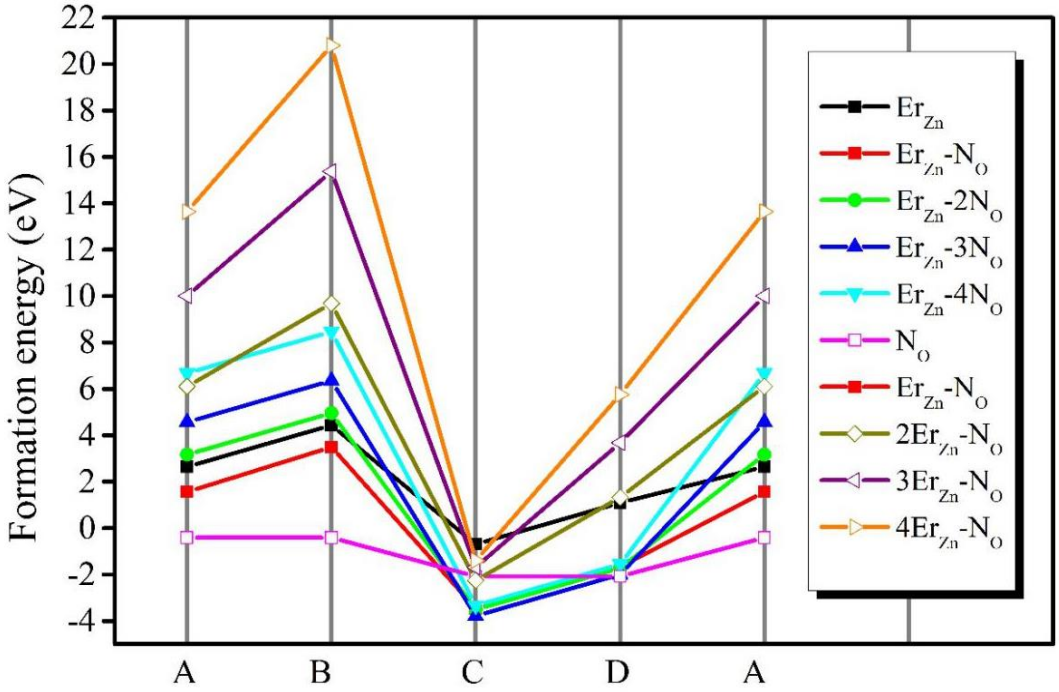

Figure S1. Effect of Chemical potential on the charge-neutral formation energies of doping systems for different extreme chemical potential conditions (case A: Zn-rich, Er-rich, case B: Zn-rich Er-poor, case C: Zn-poor, Er-poor, case D: Zn-poor, Er-rich). The formation energies under Zn-poor and Er-rich are the lowest for all the complexes, indicative of the easiest way of successfully codoping Er and N into the ZnO matrix under this condition.

Figure S1 shows charge-neutral formation energies with different dopants under the four extreme chemical potential conditions. The charge-neutral formation energies of ZnO:(Er_{Zn}-mN_O) (m=0, 1, 2, 3, 4) complexes are lower than those of ZnO:(nEr_{Zn}-N_O) (n=0, 1, 2, 3, 4) complexes, indicating that N atoms are easier to substitute the O atoms to form the Er_{Zn}-mN_O defect complexes with Er_{Zn} under the four extreme conditions. Besides, for all of the above doping complexes, growing under the Zn-poor conditions results in significantly lower formation energies than those under the Zn-rich environment, which indicates that Zn-poor crystal growth environment is more favorable for the doping process. Li et al. [S1] also found that the formation energy of Er doped ZnO under Zn-poor growth condition was lower than that of Zn-rich growth condition. The formation energies under Zn-poor and Er-rich are the lowest for all the complexes, indicative of the easiest way of successfully codoping Er

and N into the ZnO matrix under this condition.

2. Relative chemical potentials.

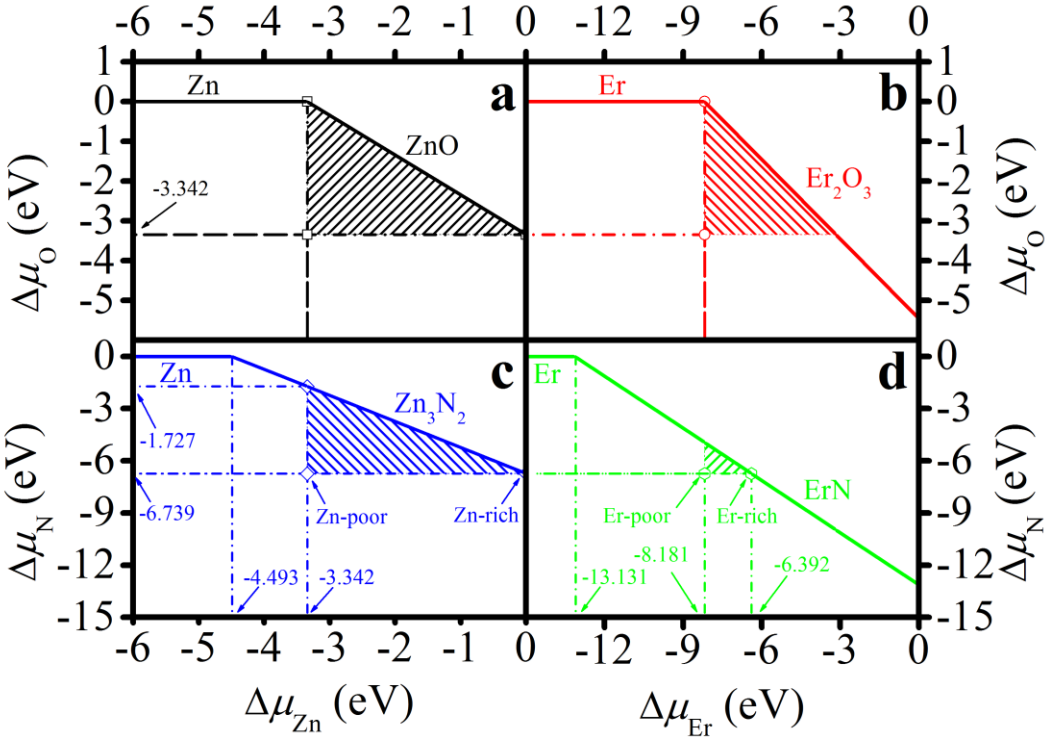

Figure S2. Relative chemical potentials $\Delta\mu_i$ (i=Zn, Er and N) by the constraint of $\Delta\mu_O$. For the doping in ZnO, four extreme conditions can be obtained from $\Delta\mu_{Zn}$, $\Delta\mu_{Er}$ and $\Delta\mu_N$ by the constraint of $\Delta\mu_O$.

Table S1. Extreme growth conditions obtained from Figure S2 by the constraint of $\Delta\mu_O$.

Constraint	$\Delta\mu_{Zn}$	$\Delta\mu_{Er}$	$\Delta\mu_O$	$\Delta\mu_N$
Zn-rich, Er-rich	0	-6.392	-3.342	-6.739
Zn-rich, Er-poor	0	-8.181	-3.342	-6.739
Zn-poor, Er-rich	-3.342	-6.392	0	-1.727
Zn-poor, Er-poor	-3.342	-8.181	0	-1.727

In order to avoid the appearance of elementary substance (Zn, O_2, Er, and N_2), the $\Delta\mu_i$ (i=Zn, O, Er, or N) should satisfy the four conditions: $\Delta\mu_{Zn}\leq 0$ eV, $\Delta\mu_O\leq 0$ eV, $\Delta\mu_{Er}\leq 0$ eV, and $\Delta\mu_N\leq 0$ eV. Meanwhile, in order to avoid the formation of competitive compounds, $\Delta\mu_i$ (i=Zn, O, Er, or N) must also satisfy the other four conditions: $\Delta\mu_{Zn}+\Delta\mu_O\leq\Delta H_f$ (ZnO), $2\Delta\mu_{Er}+3\Delta\mu_O\leq\Delta H_f$ (Er_2O_3), $3\Delta\mu_{Zn}+2\Delta\mu_N\leq\Delta H_f$ (Zn_3N_2), and $\Delta\mu_{Er}+\Delta\mu_N\leq\Delta H_f$(ErN). The formation enthalpies of ZnO, Er_2O_3, Zn_3N_2 and ErN have been calculated and the results are ΔH_f(ZnO)=-3.342 eV, ΔH_f(Er_2O_3)=-16.362 eV, ΔH_f(Zn_3N_2)=-13.479 eV and ΔH_f(ErN)=-13.131 eV, respectively. Since ZnO is used as the substrate material here, $-3.342\leq\Delta\mu_{Zn}\leq 0$ eV and $-3.342\leq\Delta\mu_O\leq 0$ eV must be satisfied firstly [see Figure S2(a)]. At the same time, due to Er and N as the doping material, $\Delta\mu_{Er}$ and $\Delta\mu_N$ are bound by them [see Figure S2(b), (c) and (d)]. The relative chemical potentials for $\Delta\mu_{Zn}$, $\Delta\mu_{Er}$, $\Delta\mu_N$, and $\Delta\mu_O$ according to their relationships, are shown in Figure S2. Four extreme conditions can be concluded from $\Delta\mu_{Zn}$, $\Delta\mu_{Er}$ and $\Delta\mu_N$ by the constraint of $\Delta\mu_O$, as displayed in Table S1 in the Supplementary Information.

3. VBM, CBM and *E*g

Table S2. VBM, CBM and E_g of the ZnO:(Er_{Zn}-mN_O) (m=0, 1, 2, 3, 4) doping systems

Defect	Er (at.%)	N (at.%)	VBM (eV)	CBM (eV)	E_g (eV)
Er_{Zn}	1.389	0	-0.225	3.056	3.281
Er_{Zn}-N_O	1.389	1.389	-2.157	1.275	3.432
Er_{Zn}-$2N_O$	1.389	2.778	-1.379	2.090	3.470
Er_{Zn}-$3N_O$	1.389	4.167	-1.493	2.015	3.507
Er_{Zn}-$4N_O$	1.389	5.556	-1.121	2.444	3.565

4. Electronic Density of States

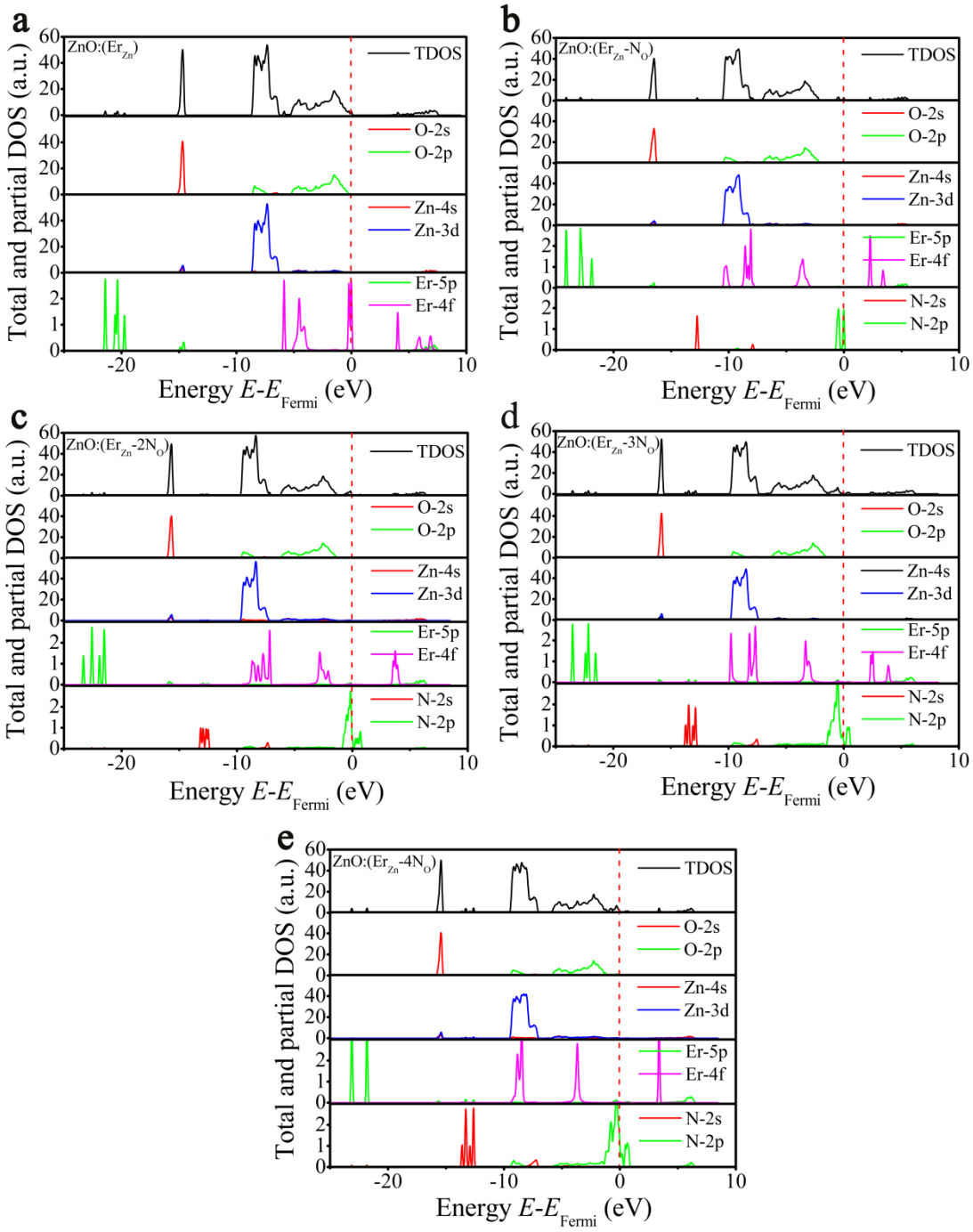

Figure S3. Density of electronic state. Total DOS (TDOS) and partial DOS (PDOS) of ZnO:(Er_{Zn}-mN_O) (m=0, 1, 2, 3, 4) calculated by GGA+U method. The Fermi level is set to zero. After doping N into the ZnO:(Er_{Zn}) matrix, the Er-4*f* states move to lower energy. With further increasing the N concentration, the hybridization between N-2*p* and Zn-3*d* states and the localization of Er-4*f* states are gradually enhanced, but the hybridization between Er-4*f* and Zn-3*d* states weakens.

The distribution of the total and partial density of states (DOS) of electrons in the ZnO:(Er_{Zn}-mN_O) (m=0, 1, 2, 3, 4) systems were calculated and shown in Figure S3, in which the Fermi level is set to zero. From Figure S3(a), it can be seen that the valence band is composed of the hybridization among the Zn-3*d*, O-2*p* and Er-4*f* states, and the VBM is mainly attributed to the O-2*p* states. The conduction band is hybridized by the Zn-4*s*, Er-5*p* and Er-4*f* states, and dominated by Zn-4*s* states. After doping N into the ZnO:(Er_{Zn}) matrix, as shown in Figure S3(b), the Er-4*f* states move to lower energy. The resonance bonding effect of the Zn-3*d* states may weaken the hybridiztion between the O-2*p* and Zn-3*d* states, thus leading the valence band toward the lower energy. On the other hand, the shift of Zn-4*s*, Er-5*p* and Er-4*f* states to the lower energy leads to the downward shift of the CBM. In addition, it can be seen that the impurity band introduced by doping N is originated by the N-2*p* states. With further increasing the N concentration, as shown Figures S3(c), (d) and (e), the hybridization between N-2*p* and Zn-3*d* states and the localization of Er-4*f* states are gradually enhanced, but the hybridization between Er-4*f* and Zn-3*d* states weakens, which may be the reason for the VBM moving to higher energy.

5. First Brillouin Zone

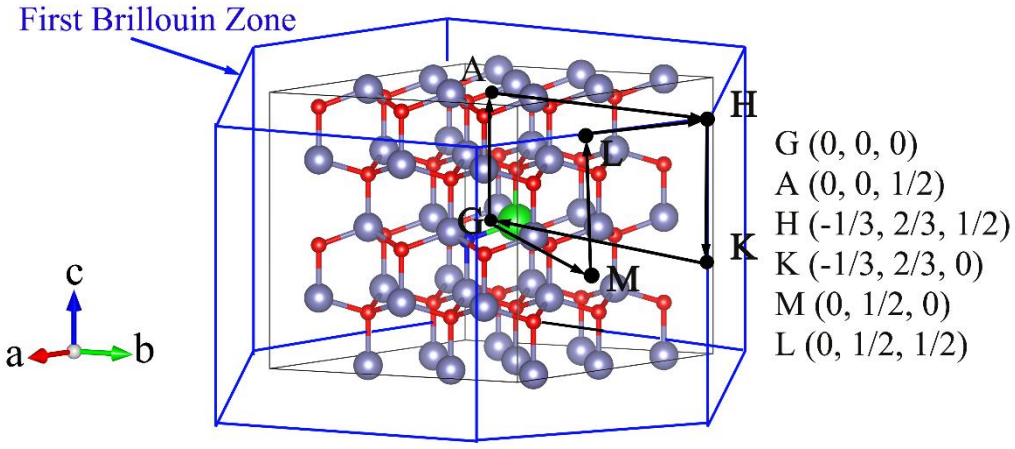

Figure S4. First Brillouin Zone. The G, A, H, K, M, and L points are marked out with coordinate values. They are Some special high symmetry points in the ZnO lattice.

6. Pair interactions

Table S3. Total energies of ZnO:(Er_{Zn}-N_O) with different Er_{Zn} and N_O distances.

Distance	1NN	2NN	3NN
Total energy (eV)	-80655.143	-80654.316	-80654.239

7. Optical properties

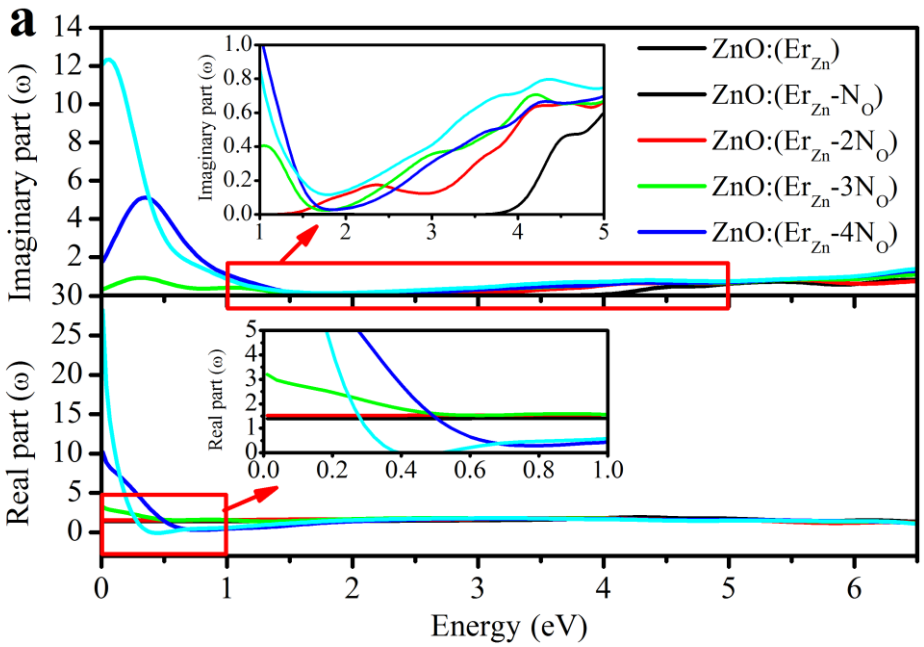

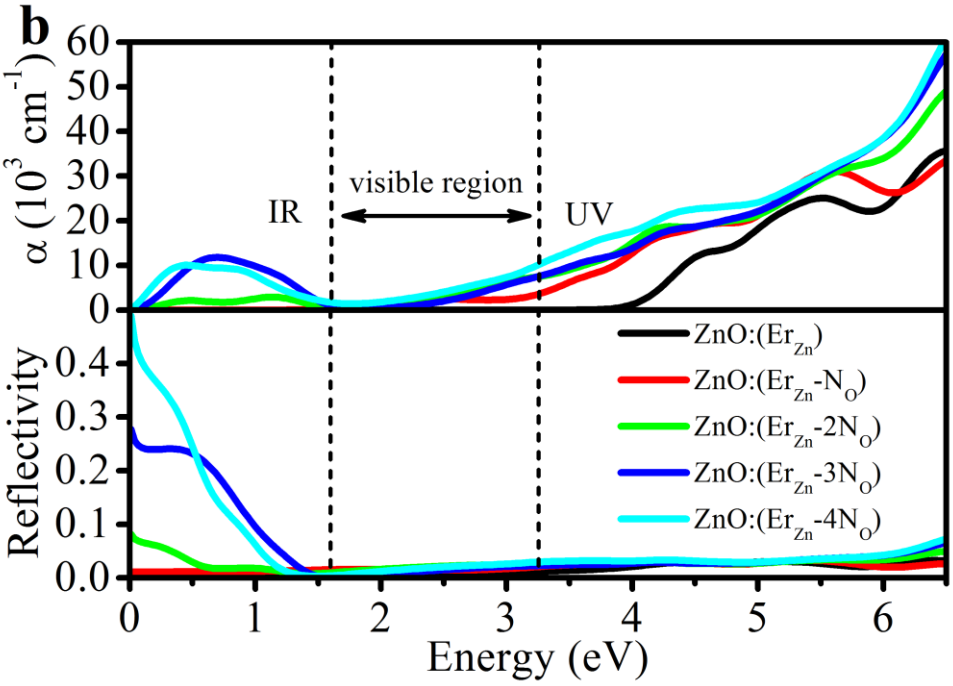

Figure S5. Optical properties. a The dielectric function of ZnO:(Er_{Zn}-mN_O) (m=0, 1, 2, 3, 4). **b** The absorption and reflectivity of ZnO:(Er_{Zn}-mN_O) (m=0, 1, 2, 3, 4). For m=2, 3, 4, there are three peaks in dielectric function curve, which originate from the transitions between the N-2*s* states and N-2*p* states, and their optical reflectivity is very high in the IR region. The optical absorption coefficient increases in both the visible and UV regions with the increasing incorporation of N atoms.

Figure S5(a) displays the dielectric function $\varepsilon(\omega)=\varepsilon_R(\omega)+i\varepsilon_i(\omega)$ of the ZnO:(Er_{Zn}-mN_O) (m=0, 1, 2, 3, 4) systems, where $\varepsilon_R(\omega)$ and $\varepsilon_i(\omega)$ are the real part and the imaginary part of the dielectric function, respectively. The imaginary part $\varepsilon_i(\omega)$ curve starts with an decreasing transition threshold with an increase in the N concentration, as 3.825, 1.466, 0, 0 and 0 eV for m=0, 1, 2, 3, and 4, respectively. For ZnO:(Er_{Zn}-mN_O) (m=2, 3, 4) systems, there are three prominent peaks with an increasing peak intensity at 0.346, 0.346, and 0.066 eV, respectively, which originate from the transitions between the N-2*s* states and N-2*p* states. This phenomenon may be

attributed to the boosted transition probability as the N concentration is increased. From the real part $\varepsilon_R(\omega)$ curve shown in Figure S5(a) and the lower inset, one can see that only the curve of ZnO:(Er_{Zn}-$4N_O$) possesses two energies with $\varepsilon_R(\omega)=0$ (0.384 eV and 0.542 eV, respectively, see the lower inset). For $\varepsilon_R(\omega)<0$ in the interval of 0.384~0.542 eV, the ZnO:(Er_{Zn}-$4N_O$) semiconductor exhibits metallic properties.

The optical absorption spectra of the ZnO:(Er_{Zn}-mN_O) (m=0, 1, 2, 3, 4) systems are predicted in Figure S5(b). The absorption edges redshift to lower energy with the increase of N concentration. This phenomenon is mainly due to the impurity band structures introduced by doping the N atoms (see Figure 3). The optical absorption coefficient increases in both the visible (1.5~3.2 eV) and ultraviolet (UV) regions with the increasing incorporation of N atoms. Moreover, the ZnO:(Er_{Zn}-mN_O) (m=2, 3, 4) systems also show considerable optical absorption in the infrared (IR) region when the concentration of N is above 1.389%. The corresponding reflectance spectra of the ZnO:(Er_{Zn}-mN_O) (m=0, 1, 2, 3, 4) systems are illustrated in Figure S5(b). The optical reflectivity of the ZnO:(Er_{Zn}-mN_O) (m=2, 3, 4) systems is very high in the IR region, which indicates that the transmittance of IR light is very low and the optical penetration of IR light will be poor for the considered materials. The optical absorption coefficient and reflectivity are both not high in the visible region for all the ZnO:(Er_{Zn}-mN_O) systems, which suggests that the transparency and penetration of the ZnO:(Er_{Zn}) film is little affected by doping N atoms.

8. P-type doping ZnO

Table S4. The doping elements for p-type doping ZnO.

Doping element	**Valent state**	**Ionic radius**	**Refs.**
Ag	1	100	S2
As	-3	222	S3
Au	1	137	S4
Be	2	31	S5
Bi	3	96	S6
C	-4	260	S7
Ce	3	103	S8

Co	3	74	S9
Cu	1	60	S10
Cs	1	169	S11
Fe	2	76	S12
K	1	133	S13
La	3	106	S14
Li	1	68	S15
Mg	2	65	S16
N	-3	171	S7
Na	1	95	S13
Nd	3	106	S17
Ni	2	72	S18
P	-3	212	S19
Sb	3	91	S20
Te	-2	221	S21
Y	3	83	S17
Yb	3	96	S17

Table S5. The codoping elements for p-type doping ZnO.

Doping element A	**Doping element B**	**Valent state (A)**	**Ionic radius (A)**	**Refs.**
Ag	N	2	97	S22
Al	N	3	50	S23
Al	P	3	50	S24
Al	C	3	50	S25
Al	As	3	50	S26
As	N	-3	222	S27
B	N	3	20	S28
Be	N	2	31	S29

C	N	-4	260	S30
Cr	C	3	64	S31
Cr	N	3	64	S32
Cu	Al	1	60	S33
Cu	N	1	60	S34
Er	K	3	88	S35
F	Li	-1	136	S36
Ga	N	3	62	S37
Ga	C	3	62	S25
Ga	P	3	62	S38
H	Li	1	10	S39
In	N	3	62	S37
In	Sb	3	62	S40
In	C	3	62	S25
Co	Li	2	74	S41
Li	P	1	68	S42
Mg	F	2	65	S43
Mg	N	2	65	S44
N	Li	-3	171	S45
N	P	-3	171	S46
Na	H	1	95	S47
Na	F	1	95	S48
P	N	-3	212	S49
S	N	-2	184	S50
S	Ag	-2	184	S51
Sb	N	3	91	S52
Sc	C	3	81	S32
Sn	N	2	102	S53
Te	N	6	56	S54

Ti	C	2	76	S31
V	N	3	74	S32
Zr	N	4	79	S26

References

[S1] H. Li, Y. Lv, J. Li, Y. Ke, *J. Alloys Comp.* **2014**, *617*, 102-107.

[S2] R. Kandulna, R. B. Choudhary, P. Maji, *J. Inorg. Org. Poly. Mater.* **2017**, *27*, 1760-1769.

[S3] T. H. Feng, X. C. Xia, *Opt. Mater. Expr.* 2017, **7**, 1281-1288.

[S4] Y. Xu, B. Yao, Y. F. Li, Z. H. Ding, J. C. Li, H. Z. Wang, Z. Z. Zhang, L. G. Zhang, H. F. Zhao, D. Z. Shen, *J. Alloys Compds.* **2014**, *585*, 479-484.

[S5] M. Chen, Y. Zhu, A. Chen, Z. Shen, Z. Tang, *Mater. Res. Bull.* **2016**, *78*, 16-19.

[S6] B. K. Singh, S. Tripathi, *J. Mater. Sci. Mater. Electr.* **2016**, *27*, 2360-2366.

[S7] W. Yu, J. Zhang, T. Peng, *Appl. Cataly. B Envir.* **2016**, *181*, 220-227.

[S8] Y. J. Liu, H. D. Zhang, X. Yan, A. J. Zhao, Z. G. Zhang, W. Y. Si, M. G. Gong, J. C. Zhang, Y. Z. Long, *RSC Adv.* **2016**, *6*. 85727-85734.

[S9] B. Henne, V. Ney, J. Lumetzberger, K. Ollefs, F. Wilhelm, A. Rogalev, A. Ney, *Phys. Rev. B* **2017**, *95*, 054406.

[S10] P. J. M. Isherwood, *Vacuum* **2017**, *139*, 173-177.

[S11] V. Ragupathi, S. Krishnaswamy, S. Sada, G. S. Nagarajan, S. Raman, *J. Mater. Sci.* **2014**, *49*, 7418-7424.

[S12] W. Zhao, X. Xiong, Y. Han, L. Wen, Z. Zou, S. Luo, H. Li, J. Su, T. Zhai, Y. Gao, Adv. Opti. Mater. **2017**, *5*, 1700146.

[S13] W. C. Au, K. Y. Chan, *Appl. Phys. A Mater. Sci. Proc.* **2017**, *123*. 485.

[S14] H. D. Zhang, M. Yu, J. C. Zhang, C. H. Sheng, X. Yan, W. P. Han, Y. C. Liu, S. Chen, G. Z. Shen, Y. Z. Long, *Nanoscale* **2015**, *7*, 10513-10518.

[S15] A. Igityan, N. Aghamalyan, S. Petrosyan, G. Badalyan, Y. Kafadaryan, *Phys. Stat. Solidi A Appl. Mater. Sci.* **2017**, *215*, 1700353.

[S16] H. Fang, J. Juang, S. Liu, *Inter. J. Nanotech.* **2017***, 14*, 992-1000.

[S17] B. Huang, *Phys. Chem. Chem. Phys.* **2017**, *19*, 12683-12711.

[S18] J. Qu, Y. Ge, B. Zu, Y. Li, X. Dou, *Small* **2016**, *12*, 1369-1377.

[S19] P. Sharma, G. Aaryashree, Vivek, S. Mukherjee, *J. Appl. Phys.* **2017**, *121*,

225306.
[S20] G. He, M. Jiang, B. Li, Z. Zhang, H. Zhao, C. Shan, D. Shen, *J. Mater. Chem. C* **2017**, *5*, 10938-10946.
[S21] Z. Yao, K. Tang, Z. Xua, J. Ma, J. Yea, S. Zhua, S. Gu, *J. Alloys Compds.* **2018**, *735*, 1232-1238.
[S22] Z. Xu, Q. Hou, L. Qu, *Inter. J. Modern Phys. B* **2017**, *31*, 1750008.
[S23] A. Ievtushenko, O. Khyzhun, I. Shtepliuk, O. Bykov, R. Jakieła, S. Tkach, E. Kuzmenko, V. Baturin, O. Karpenko, O. Olifan, *J. Alloys Compds.* **2017**, *722*, 683-689.
[S24] S. Shin, C. Kim, J. A. Lee, Y. W. Heo, J. H. Lee, J. J. Kim, *Ceram. Inter.* **2017**, *43*, 11163-11169.
[S25] H. Li, Y. Lv, H. Fu, J. Li, K. Yu, *J. Appl. Phys.* **2015**, *117*, 055701.
[S26] L. Balakrishnan, S. Gowrishankar, J. Elanchezhiyan, N. Gopalakrishnan, *Physica B* **2011**, *406*, 4447-4452.
[S27] E. Przezdziecka, E. Kaminska, K. P. Korona, E. Dynowska, W. Dobrowolski, R. Jakiela, L. Klopotowski, J. Kossut, *Sci. Tech.* **2007**, *22*, 10.
[S28] X. Chen, Z. Zhang, B. Yao, Y. Zhang, Y. Gu, P. Zhao, B. Li, D. Shen, *J. Alloys Compds.* **2016**, *672*, 260-264.
[S29] A. Chen, H. Zhu, Y. Wu, M. Chen, Y. Zhu, X. Gui, Z. Tang, *Adv. Func. Mater.* **2016**, *26*, 3696-3702.
[S30] P. Liang, C. Zhang, H. Sun, S. Liu, M. Tadé, S. Wang, *RSC Adv.* **2016**, *6*, 85727-85734.
[S31] P. J, W. S, C. Q, H. J, W. J, *Chem. Phys. Chem.* **2014**, *15*, 1611-1618.
[S32] J. Zhang, K. Tse, M. Wong, Y. Zhang, J. Zhu, *Front. Phys.* **2016**, *11*, 117405.
[S33] Y. Y. Bu, *Ceram. Inter.* **2015**, *41*, 4042-4049.
[S34] W. Ling, Z. WeiFeng, *Chin. Phys. Lett.* **2013**, *30*, 87203.
[S35] D. E. Aimouch, S. Meskine, A. Bahnes, A. Boukortt, A. Zaoui, *Optik* **2017**, *144* 539-545.
[S36] L. Cao, L. Zhu, Y. Li, M. Yang, Z. Ye, *Mater. Lett.* **2012**, *86*, 34-37.
[S37] L. Honglin, L. Yingbo, L. Jinzhu, Y. Ke, *Phys. Scripta* **2015**, *90*, 025803.
[S38] W. S. Noh, J. A. Lee, J. H. Lee, Y. W. Heo, J. J. Kim, *Ceram. Inter.* **2016**, *42*, 4136-4142.
[S39] F. Xiu, J. Xu, P. C. Joshi, C. A. Bridges, M. P. Paranthaman, *Springer* **2016**, *218*, 105-140.
[S40] M. Türker, M. Deicher, K. Johnston, H. Wolf, T. Wichert, *Hyperfine Interact.* **2015**, *231*, 65-71.
[S41] S. Ullah Awan, S. K. Hasanain, G. Hassnain Jaffari, Z. Mehmood, *Appl. Phys. Lett.* **2014**, *104*, 222906.

[S42] P. Sharma, R. Bhardwaj, R. Singh, S. Kumar, S. Mukherjee, *Appl. Phys. Lett.* **2017**, *111*, 091604.
[S43] G. Muruganandam, N. Mala, S. Pandiarajan, N. Srinivasan, R. Ramya, E. Sindhuja, K. Ravichandran, *J. Mater. Sci. Mater. Electr.* **2017**, *28*, 18228-18235.
[S44] L. Chen, Z. Xiong, Q. Wan, D. Li, *Opt. Mater.* **2010**, *32*, 1216-1222.
[S45] Y. Gai, G. Tang, J. Li, *J. Phys. Chem. Solids* **2011**, *72*, 725-729.
[S46] Y. R. Sui, B. Yao, L. Xiao, L. L. Yang, J. Cao, X. F. Li, G. Z. Xing, J. H. Lang, X. Y. Li, S. Q. Lv, *Appl. Surf. Sci.* **2013**, *287*, 484-489.
[S47] J. Li, Y. Liu, Z. Mei, L. Vines, A. Kuznetsov, X. Du, *Mater. Sci. Semiconduct. Proc.* **2017**, *69*, 28-31.
[S48] S. Deng, Z. Jiang, *Acta Phys. Sinica* **2014**, *63*, 077101.
[S49] Y. R. Sui, B. Yao, L. Xiao, L. L. Yang, J. Cao, X. F. Li, G. Z. Xing, J. H. Lang, X. Y. Li, S. Q. Lv, *Appl. Surf. Sci.* **2013**, *287*, 484-489.
[S50] W. Niu, H. Xu, Y. Guo, Y. Li, Z. Ye, L. Zhu, *Phys. Chem. Chem. Phys.* **2015**, *17*, 16705-16708.
[S51] N. X. Tian, L. Xiang, L. Zhong, Y. C. Yong, H. S. Cheng, Z. W. Hui, *Appl. Surf. Sci.* **2014**, *316*, 62-65.
[S52] T. Guo, G. Dong, Q. Chen, X. Diao, F. Gao, J. Phys. Chem. Solids **2014**, *75*, 42-47.
[S53] N. Nripasree, N. K. Deepak, *Mater. Sci. Eng. B Adv. Func. Solid State Mater.* **2016**, *211*, 121-127.
[S54] K. Tang, S. Zhu, Z. Xu, Y. Shen, J. Ye, S. Gu, *J. Alloys Compds.* **2017**, *699*, 484-488.

Methods

All calculations are carried out by the CASTEP code package [S55] based on density functional theory. It is widely used in the field of chemistry and materials science. By simulation calculation, we can get the crystal structures, formation energies, ionization energies, band structures and optical properties. It is good to predict the physical properties of the materials and provide a good way for material engineering design. The First Brillouin Zone of ZnO lattice model, and some special high symmetry points in the lattice are illustrated in Figure S4 in Supplement Information, marked out with coordinate values as G, A, H, K, M and L, respectively.

The Model of the codopants system

A 3×3×2 supercell containing 72 atoms were used for all the models in this paper. To evaluate the stability of the crystal structures, the ZnO supercell was firstly doped with one Er atom (Er_{Zn}, Er atom occupying the site of Zn atom) and one N (N_O, N atom occupying the site of O atom), in which the distances between Er_{Zn} and N_O was set as the nearest-neighbor (1NN), the second nearest-neighbor (2NN) and the third nearest-neighbor (3NN), respectively. Relaxation calculations of these ZnO:(Er_{Zn}-N_O) models were then carried out by varying the distances between the Er_{Zn} and N_O atoms. Table S2 in Supplementary Information shows the total energies of the ZnO:(Er_{Zn}-N_O) models, from which one can find that the total energy decreases slightly when the distance is decreased from 3NN to 1NN. The total energy is the lowest when the distance is located at 1NN, indicating that the Er-N codoped ZnO is most stable at 1NN position. Therefore, Er-N codoped ZnO at 1NN position is used for the dopants in the following of this work.

For the codoped systems, different Er and N concentrations play important roles on the stability of the models. In order to obtain representative codoping systems effectively in our study, some special models of ZnO:(Er_{Zn}), ZnO:(N_O), ZnO:($2Er_{Zn}$), ZnO:(Er_{Zn}-N_O), ZnO:($2N_O$), ZnO:($3Er_{Zn}$), ZnO:($2Er_{Zn}$-N_O), ZnO:(Er_{Zn}-$2N_O$), ZnO:($3Er_{Zn}$-N_O), ZnO:($2Er_{Zn}$-$2N_O$), ZnO:(Er_{Zn}-$3N_O$), ZnO:($4Er_{Zn}$-N_O), ZnO:($3Er_{Zn}$-$2N_O$), ZnO:($2Er_{Zn}$-$3N_O$), and ZnO:(Er_{Zn}-$4N_O$) were constructed and their formation enthalpies were calculated. The results are shown in Figure 1(b). It is obvious that the formation enthalpies vary linearly with the concentration of N for the complexes with same number of total dopants. So two representative codoping complexes [ZnO:(Er_{Zn}-mN_O) (m=0, 1, 2, 3, 4) and ZnO:(nEr_{Zn}-N_O) (n=0, 1, 2, 3, 4)] were proposed and studied to evaluate the structural, electronic, and optical properties of the Er-N codoping in ZnO in this work. ZnO:(Er_{Zn}-mN_O) (m=0, 1, 2, 3, 4) [ZnO:(nEr_{Zn}-N_O) (n=0, 1, 2, 3, 4)] corresponds to concentration of the N (Er) dopants of 0 at.%, 1.389 at.%, 2.778 at.%, 4.167 at.% and 5.556 at.% for different m (n), respectively. Figure 1(a) shows partial view of the models considered in this work.

Defect formation energies and ionization energies

Defect formation energy of each system is defined by the formula as follows:

$$\Delta E_f(\alpha, q) = E_t(\alpha, q) - E_t(\mathrm{ZnO}) - \sum_i n_i(\mu_i + \Delta\mu_i) + q[E_{Fermi} + E_{VBM}(\mathrm{ZnO}) + \Delta V] \quad (1)$$

where $E_t(\alpha, q)$ is the total energy of the system containing defect α and charge q, and E_t(ZnO) is the total energy of the intrinsic ZnO bulk material. n_i is the atom number of

element i (i = Zn, Er, O or N) that is added to ($n_i > 0$) or removed from ($n_i < 0$) the intrinsic ZnO bulk material. μ_i is the chemical potential of element i. $\Delta\mu_i$ is the relative chemical potential of element i which is determined by the relationship as follows: $\Delta\mu_i=\mu_i$(compound)$-\mu_i$(elementary substance). E_{Fermi} is the Fermi level of the system with its value varying between valence band maximum (VBM) and conduction band minimum (CBM), namely the bandgap (E_g). E_{VBM}(ZnO) is the VBM energy of the intrinsic ZnO. ΔV is the correction potential introduced to describe the electrostatic potential difference between the supercells with and without a dopant impurity.

In the first-principles calculations, ionization energy $\varepsilon(q/q')$ of a semiconductor material can be described by Eq. (2) and defined as the Fermi energy [E_{Fermi} in Eq. (1)] when the defect formation energy $\Delta E_f(\alpha, q)$ of the system with a defect α and charge q is equal to that of the defect α but with another charge q'. From Eq. (2), it is obvious that the ionization energy $\varepsilon(q/q')$ is independent on the chemical potential μ_i of each element i.

$$\varepsilon(q/q') = \frac{E_t(\alpha,q) - E_t(\alpha,q') + q\Delta V - q'\Delta V'}{q'-q} - E_{VBM}(\mathrm{ZnO}) \qquad (2)$$

Chemical potentials

From the Eq. (1), it can be seen that the defect formation energy $\Delta E_f(\alpha, q)$ is closely related with the μ_i and $\Delta\mu_i$ of each element i, of which μ_i and $\Delta\mu_i$ also need to be determined. Under specific thermodynamic equilibrium conditions, μ_i and $\Delta\mu_i$ are both limited by the growth conditions. The value of μ_i is determined by total energy of gas or solid formed by element i. Specifically, $\mu_{Zn}=E_t$(Zn), $\mu_{Er}=E_t$(Er), $\mu_O=1/2E_t(O_2)$, $\mu_N=1/2E_t(N_2)$, where E_t(Zn) and E_t(Er) are the total energies of Zn and Er solids, respectively, and $E_t(O_2)$ and $E_t(N_2)$ are the total energies of oxygen and nitrogen molecules placed in the 15×15×15 Å^3 cube, respectively. $\Delta\mu_i$ is the relative chemical potential of element i in a particular environment, and can be calculated by the formula: $\Delta\mu_i=\mu_i$(compound)$-\mu_i$, where μ_i(compound) is the chemical potential of element i in a specific compound. However, the value of $\Delta\mu_i$ cannot be gained directly because μ_i(compound) cannot be calculated directly. But $\Delta\mu_i$ can be obtained to be limited in a particular range by the constraints of formation enthalpies and bulk thermodynamic equilibrium conditions.

References

[S55] M. D. Segall, P. J. D. Lindan, M. J. Probert, C. J. Pickard, P. J. Hasnip, S. J. Clark, M. C. Payne, *J. Phys.: Condens. Matter* **2002**, *14*, 2717–2744 .

Data availability

The datasets generated during and/or analyzed during the current study are available from the corresponding author on reasonable request.